EFFECT OF GAS PRESSURE AND FILM THICKNESS ON THE OPTICAL CONSTANTS OF TRANSPARENT CONDUCTING OXIDE BASED ON ZINC OXIDE

© 2016 **M. M. Abd El-Raheem[*,**]; A. K. Diab[**]; Abdullah Alhuthali[*]; Ateyyah M. Al-Baradi[*]**

[*]Faculty of science, Taif University, Taif 888, Saudi Arabia
[**]Faculty of science, Sohag University, Sohag 82524, Egypt

Corresponding author: M. M Abd El-Raheem

E-mail: elneh@yahoo.com

Thin films of aluminum zinc oxide are prepared using DC magnetron sputtering. It was found that changing the thickness of the film as well as the pressure of argon affect the transmittance, optical gap, width of the band tails of the localized state, refractive index, real and imaginary parts of the dielectric function. The real and imaginary parts of optical conductivity as well as volume and surface energy loss functions are investigated in the light of changing the thickness of the films and argon pressure.

Keywords: *thin film, sputtering, optical energy gap, refractive index, optical conductivity.*

OCIS codes: 170.5810

Submitted 11.03.2015

1. Introduction

Transparent conductive zinc oxide thin films have been investigated because of their good electrical and optical properties in addition to their large band gap, abundance in nature and absence of toxicity. The properties of ZnO thin films depend on the non-stoichiometry of the films, resulting from the presence of oxygen vacancies and interstitial zinc [1]. Besides, aluminum-doped zinc oxide (AZO) films can be deposited at relatively low deposition temperature [2, 3] with good stability [4]. The electrical behavior of ZnO thin films could be improved by replacing Zn ions species by elements with higher valence, such as In, Al or Ga [5] using the metal-organic chemical vapor deposition method [4], the sol–gel method [6], spray pyrolysis [7], pulsed laser deposition [8] or sputtering [9]. The electrical and optical properties are dependent on the deposition [10] and post deposition condition [11], because these properties change with the absorption and desorption of oxygen that occurs during these processes. Aluminum-doped zinc oxide ceramics with 0–2.5 mas % alumina (Al_2O_3) content were prepared using a solid-state reaction technique. It was found that aluminum zinc oxide grains became finer in size and more irregular in shape than undoped ZnO as the Al_2O_3 content increased [12]. Aluminum-doped zinc oxide polycrystalline thin films were prepared by sol–gel dip-coating process on optical glass substrates [13]. It was found that with the annealing temperature from 300 to 500 °C, the film was oriented along the (002) direction, the grain size of the film increased, the transmittance also became higher and the electrical resistivity decreased. Kim and coworkers reported that 0.8 at % Al was the optimal concentration in order to obtain the lowest resistivity in AZO samples grown using the PLD technique [14]. As for the target materials, usually the composite target sintered ceramic $ZnO:Al_2O_3$ (98:2) target is used for RF sputtering [15]. Alloy target containing 1.5 mas % Al in Al-Zn is also used as the target material for AZO growth [16]. The reported resistivity of AZO varies greatly from 9.8×10^{-2} to 1.5×10^{-4} Ω cm, resulting from different deposition conditions [17–20]. The characteristics of AZO thin films can be adjusted by adequate doping processes where, AZO thin films have been prepared on glass substrates using a sol–gel route and the radio-frequency magnetron sputtering process [21]. It was found that stoichiometry could be easily adjusted by controlling then anosized precursor concentration and the thickness by dip-coating cycles. In addition, the AZO (2 at % Al) films exhibited the hexagonal wurzite structure with (002) preferred crystal orienta-

tion. Nanocrystalline AZO thin films have been prepared by reactive RF-magnetron sputtering, the AFM result shows that the grain size of the un-doped ZnO film is larger than that of 4 mas % Al-doped ZnO film, suggesting that the particles in ZnO films become smaller with increasing Al-contents [22]. It was found also that the optical transmittance of AZO thin films was not influenced by RF-power. It was reported that the maximum value of the transmittance of AZO thin films deposited using magnetron sputtering were in the range from 85 to 90% depending on the condition of preparation [23].

This work is intended to study the effect of changing the pressure of argon and thickness of the thin films on the optical properties of aluminum zinc oxide Al_2ZnO_4.

2. Methodology

The thin films under test (Al doped ZnO thin films) were deposited on a pre-cleaned glass substrate using UNIVEX 350 SPUTTERING UNIT with DC POWER MODEL Turbo drive TD20 classic (Leybold), and rate thickness monitor model INFICON AQM-160. The Al_2ZnO_4 target was purchesed from Catheyand used as a sputtering source. The mass ratio of Al_2O_3 to ZnO (both were 99.99% purity) was 20%. The high vacuum of the chamber was better than 2×10^{-6} Torr and sputtering was carried out in argon (99.999%) atmosphere of 5×10^{-2} Torr. The substrate temperature was kept at 25 °C during deposition. The target-substrate distance was 10 cm with an angle of 65°. The rate of deposition was 15 sc/cm. A set of films was prepared under different pressure of argon (5×10^{-2}, 10×10^{-2}, 15×10^{-2}, 20×10^{-2}, 50×10^{-2} Torr). Another set of films was prepared with different thickness (300, 400, 500, 600, 700 and 800 nm). The structural characteristics of Al_2ZnO_4 thin films were investigated by X-ray diffraction pattern. Philips X-ray diffractometer model X′ Pert was used for the measurements which utilized monochromatic CuK_α = 1.5406 Å and radiation operated at 40 kV and 25 mA. The diffraction patterns were recorded automatically with scanning speed of 2 deg/min. The optical transmittance and absorbance of the films were measured in the wavelength range of 200–1200 nm at normal incidence by using double beam spectrophotometer (JASCO model V-670 UV-VIS-NIR).

3. Results and discussions

3.1. Effect of argon pressure and thickness of the films on the optical gap, Urbach tails, refractive index, carrier concentrations

The variations of both transmittance and reflectance with the incident wavelength of Al_2ZnO_4 thin films deposited under different pressure of argon are demonstrated in Fig. 1a. It is clear that the behavior of the reflectance is reversing that of the transmittance. Also, it is obvious that the maximum value of the transmittance of all the films is 85% and shifted toward the longer wavelength with increasing the pressure of the gas. Besides, the minimum value of the reflectance for the films under test is 10%. On the other hand, the transmittance and reflectance of the films of different thicknesses are shown in Fig. 1b indicating that the number

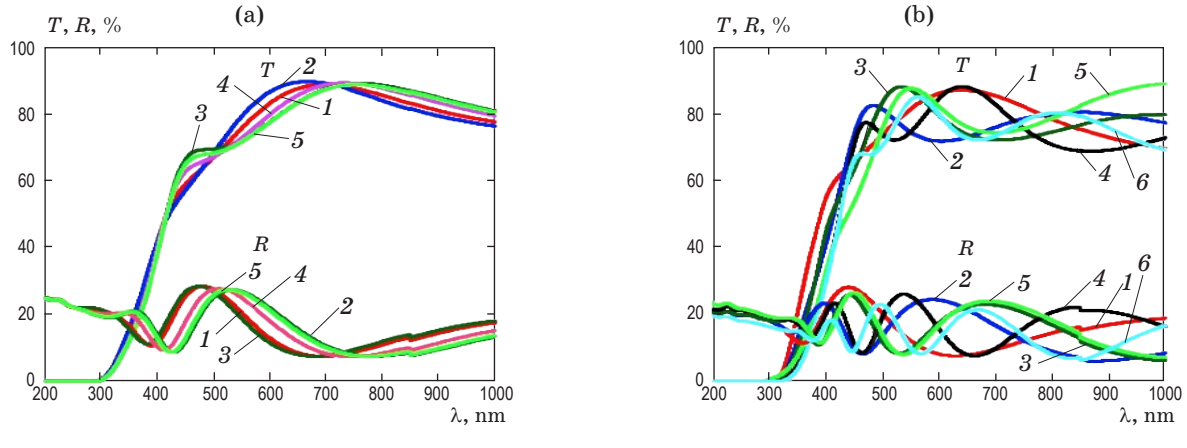

Fig. 1. Spectra of transmittance and reflectance for Al_2ZnO_4 thin films deposited under different pressures of argon (a: *1* – 5×10^{-2}, *2* – 10×10^{-2}, *3* – 15×10^{-2}, *4* – 20×10^{-2}, *5* – 25×10^{-2} Torr) and for different thicknesses (b: *1* – 300, *2* – 400, *3* – 500, *4* – 600, *5* – 700, *6* – 800 nm).

of interference fringes increases with increasing the film thickness confirming the best surface quality and homogeneity of the film [24]. The maximum value of the transmittance was found to be 85% for all the films of the considered set, and these maxima are shifted toward the longer wavelength too. The allowed indirect optical energy gap E_{op} was estimated from optical measurements using the following expression [25]:

$$(\alpha h\nu)^{1/2} = A(h\nu - E_{op}), \quad (1)$$

where α is the absorption coefficient, ν is the frequency of the incident wavelength, h is Plank's constant. The values of the allowed indirect optical energy gap E_{op} for both of the two sets of the films can be obtained from the plots of $(\alpha h\nu)^{1/2}$ versus $(h\nu)$ by extrapolating the linear portion of the plots of $(\alpha h\nu)^{1/2}$ versus to $(h\nu) = 0.0$ as shown in Figs. 2a, b respectively. The optical gap of the prepared films under different pressure were 3.7, 3.88, 4.88, 3.9, and 3.98 eV for the films prepared under the pressures 5×10^{-2}, 10×10^{-2}, 15×10^{-2}, 20×10^{-2}, 25×10^{-2} Torr respectively revealing that E_{op} increases with increasing the gas pressure as shown in Fig 2a. This increase in the optical band gap can be explained by the Burstein-Mosse effect [26] caused by an increased free-carrier concentration with a decrease in Ar pressure. The optical gap of the other set of films are 3.82, 3.84, 3.86, 3.86, and 3.9 eV for the films of thicknesses 300, 400, 500, 600, and 700 nm respectively as seen in Fig. 2b indicating that the optical gap increases with increasing the film thickness. This can be attributed to the improvement in the crystals, in morphological changes of the films, in changes of atomic distances and grain size and structural defects in the films [23].

The Urbach tails (width of the band tails of the localized states) E_u, that represents the degree of disorder in an amorphous semiconductor for Al_2ZnO_4 thin films prepared under different argon pressure can be obtained using the expression

$$\alpha = \alpha_0 \exp(h\nu/E_u). \quad (2)$$

E_u is estimated from the slopes of the straight lines of the relation (plot lnα versus $(h\nu)$ as shown in Fig. 3a. The results of Urbach tails reveal that E_u has the same value of 0.69±0.02 eV within the experimental error for all the considered films. Concerning the set of films of different thicknesses, Urbach results estimated from Fig. 3b were 0.400, 0.457, 0.445, 0.471, 0.712 and 0.456 eV for the films with thicknesses of 300, 400, 500, 600, 700, and 800 nm respectively. It is noticed that the film with a thickness of 700 nm has an extremely higher value of E_u than those of the other films.

The refractive index can be estimated using the following equation [27]:

$$n = (1 + R)/(1 - R) + [4R/(R - 1)^2 - k^2]^{1/2}. \quad (3)$$

Fig. 4 represents the variation of the refractive index with photon energy for both of the two sets of the films under test. It is clear that the refractive indices have the normal dispersion; in addition, the refractive indices have the trend to increase with increasing both of argon pressure and film thickness, due to increasing the thickness as a result of increasing the pressure of the gas.

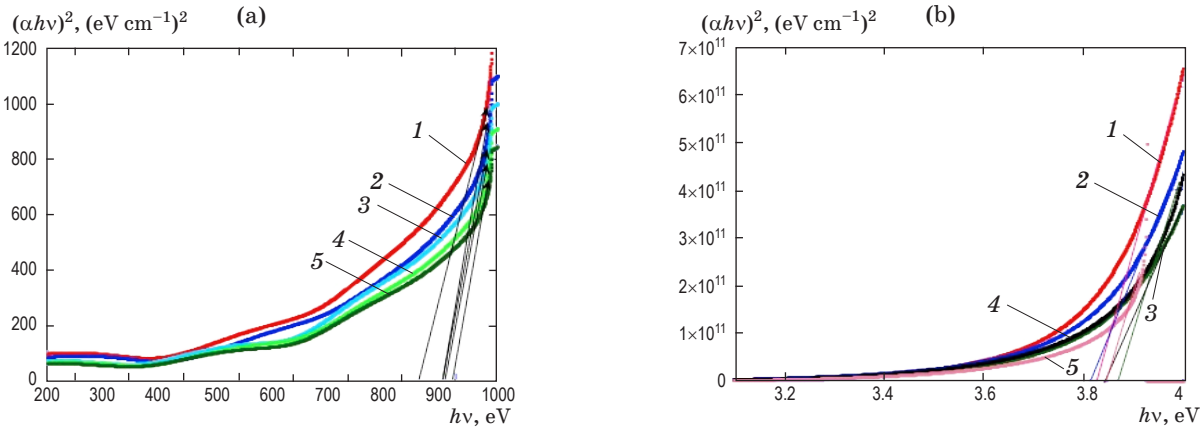

Fig. 2. Plots of $(\alpha h\nu)^2$ vs. photon energy for as-prepared Al_2ZnO_4 thin films at different argon pressure (a: *1* – 5×10^{-2}, *2* – 10×10^{-2}, *3* – 15×10^{-2}, *4* – 20×10^{-2}, *5* – 25×10^{-2} Torr) and for different thicknesses (b: *1* – 300, *2* – 400, *3* – 500, *4* – 600, *5* – 700 nm).

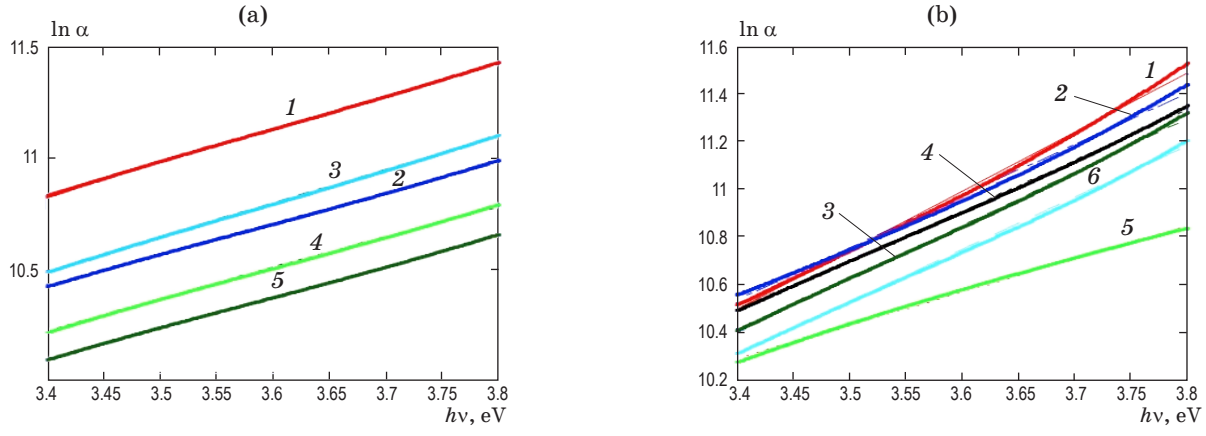

Fig. 3. Plots of lnα vs. photon energy for as-prepared Al_2ZnO_4 thin films at different pressure of argon gas (a: *1* – 5×10^{-2}, *2* – 10×10^{-2}, *3* – 15×10^{-2}, *4* – 20×10^{-2}, *5* – 25×10^{-2} Torr) and for different thicknesses (b: *1* – 300, *2* – 400, *3* – 500, *4* – 600, *5* – 700, *6* – 800 nm).

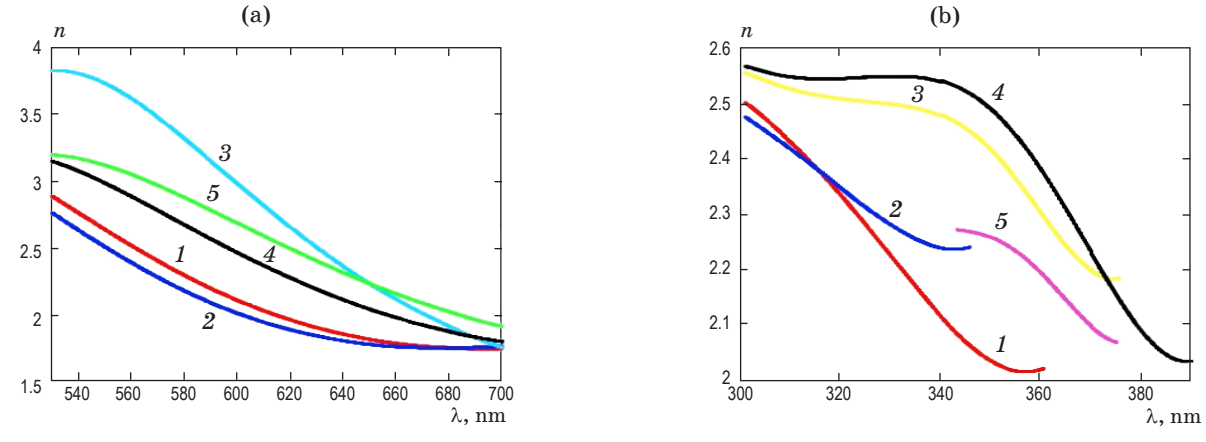

Fig. 4. Spectra of refractive index n for Al_2ZnO_4 thin films deposited under different pressure of argon (a: *1* – 5×10^{-2}, *2* – 10×10^{-2}, *3* – 15×10^{-2}, *4* – 20×10^{-2}, *5* – 25×10^{-2} Torr) and for different thicknesses (b: *1* – 300, *2* – 400, *3* – 600, *4* – 700, *5* – 800 nm).

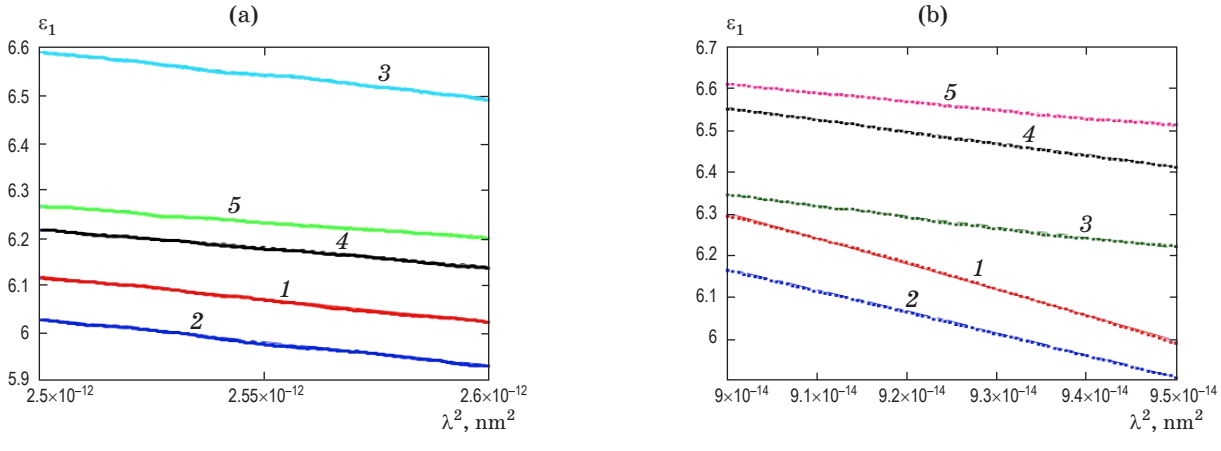

Fig. 5. Plots of ε_1 vs. λ^2 for Al_2ZnO_4 thin films deposited under different pressure of argon (a: *1* – 5×10^{-2}, *2* – 10×10^{-2}, *3* – 15×10^{-2}, *4* – 20×10^{-2}, *5* – 25×10^{-2} Torr) and for different thicknesses (b: *1* – 300, *2* – 400, *3* – 600, *4* – 700, *5* – 800 nm).

The carrier concentration N can be obtained using the equation [28]

$$\varepsilon_1 = n^2 = \varepsilon_L - \frac{e^2 N}{4\pi\varepsilon_0 m^* c^2}\lambda^2, \quad (4)$$

where e is the elementary charge, ε_0 is the permittivity of free space, N/m^* is the real part of the dielectric constant, ratio of free carrier concentration to the effective mass, ε_L is the lattice dielectric constant. The plots of ε_1 vs. λ^2 for the two sets of the films under test are shown in Fig. 5. The carrier concentrations were calculated from the slope of the straight lines. The values of N were found to be 3.34×10^{25}, 3.53×10^{25}, 3.50×10^{25}, 2.86×10^{25} and 2.39×10^{25} m^{-3} for the films deposited under the pressures 5×10^{-2}, 10×10^{-2}, 15×10^{-2}, 20×10^{-2} and 25×10^{-2} Torr respectively. Excepting the film deposited under pressure 5×10^{-2} Torr, it can be said that the free carrier concentration decreases with increasing the pressure of the gas, which can be owed to the decrease of the grain size with increasing the pressure [29]. On the other side, the values of N belonging to the second set of films were found to be 2.19×10^{26}, 1.83×10^{26}, 9.01×10^{26}, 10.08×10^{26}, and 7.19×10^{26} m^{-3} for the films of thicknesses 300, 400, 600, 700, and 800 nm respectively. This indicates that the carrier concentration has the tendency to increase with increasing the film thickness.

3.2. Effect of gas pressure and film thickness on the loss factor, optical conductivity, loss energy factor

The complex dielectric constant $\varepsilon(h\nu)$ is described by [30]

$$\varepsilon(h\nu) = \varepsilon_1(h\nu) - \varepsilon_2(h\nu), \quad (6)$$

$$\tan\delta = \varepsilon_2/\varepsilon_1, \quad (7)$$

where $\varepsilon_1 = n^2 - k^2$ is the real, $\varepsilon_2 = 2nk$ is the imaginary parts of the dielectric constant and $\tan\delta$ is the loss factor. The variation in the loss factor with photon energy is displayed Fig. 6. It is clear from the figure that dissipation factor increases with increasing the frequency. The real σ_1 and imaginary σ_2 components of optical conductivity are described as [31]

$$\sigma_1 = \omega\varepsilon_2\varepsilon_0,\ \sigma_2 = \omega\varepsilon_1\varepsilon_0, \quad (8)$$

where ω is the angular frequency, ε_0 is the permittivity of free space. The spectra of real and imaginary parts of the optical conductivity are shown in Fig. 7. It is seen that the real part of the optical conductivity σ_1 increases by increasing photon energy which is owed to increasing the electrons excited by photon energy [31].

The volume (bulk) energy loss function (VELF) and the surface energy loss function (SELF) are related to the real and imaginary parts of the dielectric constants by the relations [32]

$$\text{VELF} = \frac{\varepsilon_2^2}{\varepsilon_1^2 - \varepsilon_2^2}, \quad (10)$$

$$\text{SELF} = \frac{\varepsilon_2^2}{(\varepsilon_1 + 1)^2 + \varepsilon_2^2}. \quad (11)$$

The distribution of the volume and surface energy loss of the two sets of films as a function of the photon energy are shown in Fig. 8. The observed dispersion behavior can be explained if it is assumed to be the response of a set of Lorentzian oscillators of adjustable strength and position [33].

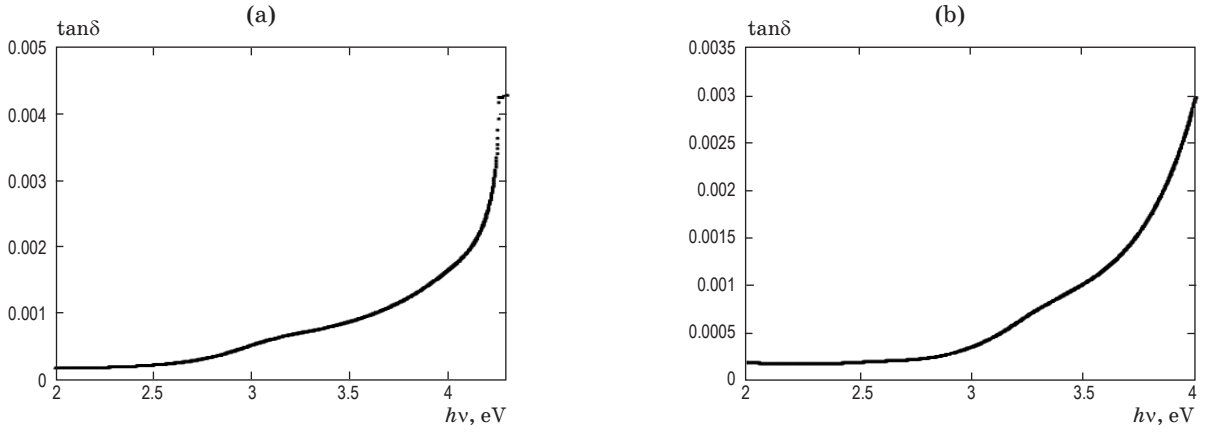

Fig. 6. Variations of average loss factor tan δ with photon energy for Al_2ZnO_4 thin films deposited under different pressure of argon (a) and variations of the mean loss factor with photon energy for the as-prepared Al_2ZnO_4 thin films (b).

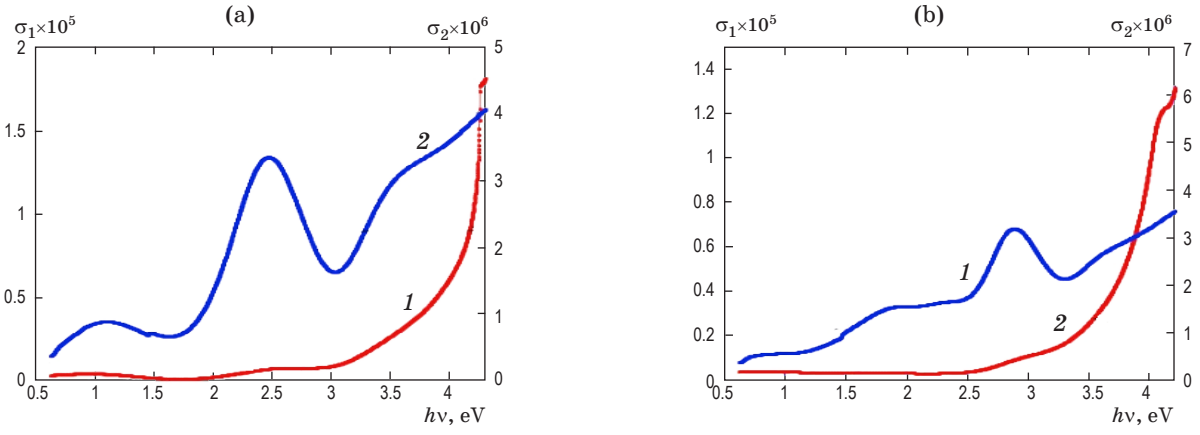

Fig. 7. Changes of the mean value of the real (*1*) and imaginary (*2*) parts of the optical conductivity with photon energy for Al_2ZnO_4 thin films deposited under different pressure of argon (a) and for different thicknesses (b).

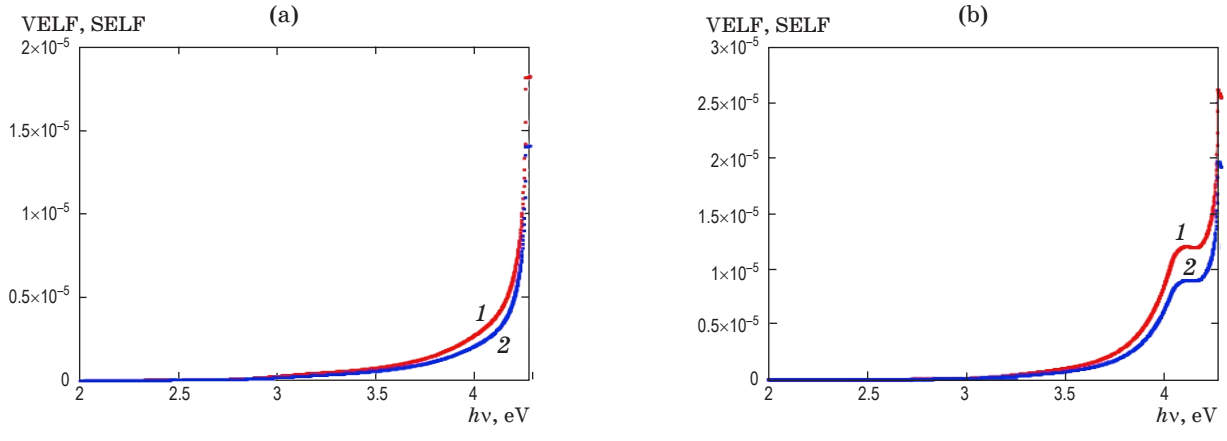

Fig. 8. Distributions of the mean value of the volume and the surface energy for Al_2ZnO_4 thin films deposited under different pressure of argon (a) and for different thicknesses (b). VELF – *1*, SELF – *2*.

4. Conclusions

Our results reveal that, the maximum value of the transmittance was 80%. The optical energy gap increases with increasing both of the gas pressure and thickness of the film. Urbach tails were found to increase with film thickness. The refractive index has a normal dispersion. The carrier concentration decreases with increasing argon pressure and tends to increase with increasing the film thickness. The real and imaginary parts of the optical conductivity as well as the loss factor increase with increasing gas pressure. Both of the volume and surface energy loss increases with photon energy.

* * * * *

ЛИТЕРАТУРА

1. *Major S., Chopra K.L.* Indium-doped zinc oxide films as transparent electrodes for solar cells // Sol. Energy Mater. 1988. V. 17. № 5. P. 319–327.

2. *Zhang D.H., Yang T.L., Ma J., Wang Q.P., Gao R.W., Ma H.L.* Preparation of transparent conducting ZnO:Al films on polymer substrates by rf magnetron sputtering // Appl. Surf. Sci. 2000. V. 158. № 1. P. 43–48.

3. *Minami T., Sonohara H., Takata S., Sato H.* Highly transparent and conductive zinc-stannate thin films prepared by RF magnetron sputtering // Jap. J. Appl. Phys. 1994. V. 33. № 12. P. 1693.

4. *Lau W.S., Fonash S.J.* Highly transparent and conducting zinc oxide films deposited by activated reactive evaporation // J. Elec. Mater. 1987. V. 16. № 3. P. 141–149.

5. *Nunes P., Fortunato E., Martins R.* Influence of the post-treatment on the properties of ZnO thin films // Thin Solid Films. 2001. V. 383. № 1. P. 277–280.

6. *Hu J., Gordon R. G.* Textured aluminum-doped zinc oxide thin films from atmospheric pressure chemical-vapor deposition // J. Appl. Phys. 1992. V. 71. № 2. P. 880–890.

7. *Natsume Y., Sakata H.* Zinc oxide films prepared by sol-gel spin-coating // Thin solid films. 2000. V. 372. № 1. P. 30–36.

8. *Lokhande B.J., Uplane M.D.* Structural, optical and electrical studies on spray deposited highly oriented ZnO films // Appl. Surf. Sci. 2000. V. 167. № 3 . P. 243–246.

9. *Bose S., Ray S., Barua A.K.* Textured aluminium-doped ZnO thin films prepared by magnetron sputtering // J. Phys. D: Appl. Phys. 1996. V. 29. № 7. P. 1873.

10. *Ellmer K.* Magnetron sputtering of transparent conductive zinc oxide: Relation between the sputtering parameters and the electronic properties // J. Phys. D: Appl. Phys. 2000. V. 33. № 4. P. 17.

11. *Nunes P., Fernandes B., Fortunato E., Vilarinho P., Martins R.* Performances presented by zinc oxide thin films deposited by spray pyrolysis // Thin Solid Films. 1999. V. 337. № 1. P. 176–179.

12. *Chou Y.H., Chau J.L.H., Wang W.L., Chen C.S., Wang S.H., Yang C.C.* Preparation and characterization of solid-state sintered aluminum-doped zinc oxide with different alumina contents // Bull. Mater. Sci. 2011. V. 34. № 3. P. 477–482.

13. *Zhou H.M., Yi D.Q., Yu Z.M., Xiao L.R., Li J.* Preparation of aluminum doped zinc oxide films and the study of their microstructure, electrical and optical properties // Thin Solid Films. 2007. V. 515. № 17. P. 6909–6914.

14. *Kim H., Pique A., Horwitz J.S., Murata H., Kafafi Z.H., Gilmore C. M., Chrisey D.B.* Effect of aluminum doping on zinc oxide thin films grown by pulsed laser deposition for organic light-emitting devices // Thin Solid Films. 2000. V. 377. P. 798–802.

15. *Fortunato E., Nunes P., Marques A., Costa D., Águas H., Ferreira I., Martins R.* Transparent, conductive ZnO:Al thin film deposited on polymer substrates by RF magnetron sputtering // Surf. Coat. Tech. 2002. V. 151. P. 247–251.

16. *Ko M., Song P.K., Shigesato Y., Frach P., Mizukami A., Suzuki K.* Al-doped ZnO films deposited by reactive magnetron sputtering in mid-frequency mode with dual cathodes // Jap. J. Appl. Phys. 2002. V. 41. № 2. P. 814.

17. *Jeong S.H., Lee J.W., Lee S.B., Boo J.H.* Deposition of aluminum-doped zinc oxide films by RF magnetron sputtering and study of their structural, electrical and optical properties // Thin Solid Films. 2003. V. 435. № 1. P. 78–82.

18. *Hong R.J., Jiang X., Szyszka B., Sittinger V., Pflug A.* Studies on ZnO:Al thin films deposited by in-line reactive mid-frequency magnetron sputtering // Appl. Surf. Sci. 2003. V. 207. № 1. P. 341–350.

19. *Kim H., Horwitz J.S., Qadri S.B., Chrisey D.B.* Epitaxial growth of Al-doped ZnO thin films grown by pulsed laser deposition // Thin Solid Films. 2002. V. 420. № 107. P. 111.

20. *Fang G., Li D., Yao B.L.* Fabrication and vacuum annealing of transparent conductive AZO thin films prepared by DC magnetron sputtering // Vacuum. 2002. V. 68. № 4. P. 363–372.

21. *Wu G.M., Chen Y.F., Lu H.C.* Aluminum-doped zinc oxide thin films prepared by sol-gel and RF magnetron sputtering // VIII Inter. Conf. 2010. P. 34.

22. *Bidmeshkipour S.Shahtahmasebi N.* Different properties of aluminum doped zinc oxide nanostructured thin films prepared by radio frequency magnetron sputtering // Semiconductors. 2013. V. 47. № 6. P. 787–790.

23. *Al-Ofi H.H., El-Raheem M.M., Al-Baradi A.M., Atta A.A.* Structural and optical properties of Al_2ZnO_4 thin films deposited by DC sputtering technique // J. Non-Oxide Glasses. 2012. V. 3. № 3. P. 39–54.

24. *Abd El-Raheem M.M., Ali H.M., El-Husainy N.M.* Characterization of electron beam evaporated CdTe thin films for optoelectronic devices // J. Optoelec. Adv. Mater. 2009. V. 11. № 6. P. 813–819.

25. *Pal U., Samanta D., Ghorai S., Chaudhuri A.K.* Optical constants of vacuum-evaporated polycrystalline cadmium selenide thin films // J. Appl. Phys. 1993. V. 74. № 10. P. 6368–6374.

26. *Steckl A.J., Mohammed G.* The effect of ambient atmosphere in the annealing of indium tin oxide films // J. Appl. Phys. 1980. V. 51. № 7. P. 3890–3895.

27. *El-Nahass M.M., Atta A.A., El-Sayed H.E.A., El-Zaidia E.F.M.* Structural and optical properties of thermal evaporated magnesium phthalocyanine (MgPc) thin films // Appl. Surf. Sci. 2008. V. 254. № 8. P. 2458–2465.

28. *El-Nahass M.M., El-Deeb A.F., Metwally H.S., Hassanien A.M.* Structural and optical properties of iron (III) chloride tetraphenylporphyrin thin films // Eur. Phys. J. Appl. Phys. 2010. V. 52. № 1. P. 10403.

29. *Kwak D.J., Park K.I., Kim B.S., Lee S.H., Lee S.J., Lim D.G.* Argon gas pressure and substrate temperature dependences of ZnO:Al film by magnetron sputtering // J. Kor. Phys. Soc. 2004. V. 12. № 1. P. 23–43.

30. *El-Nahass M.M., Atta A.A., El-Raheem M.M., Hassanien A.M.* Structural and optical properties of DC sputtered Cd_2SnO_4 nanocrystalline films // J. Alloy. Comp. 2014. V. 585. P. 1–6.

31. *Caglar Y., Ilican S., Caglar M.* Single-oscillator model and determination of optical constants of spray pyrolyzed amorphous SnO_2 thin films // Euro. Phys. J. B-Cond. Matt. Comp. Syst. 2007. V. 58. № 3. P. 251–256.

32. *Pankove J.* Optical Processes in Semiconductors. Courier Corporation, 2012.

33. *Krishna M.G., Pillier J.S., Bhattacharya A.K.* Variable optical absorption edge in ion beam sputtered thin ytterbium oxide films // Thin Solid Films. 1999. V. 357. № 2. P. 218–222.